Four-Wavelength Near-Infrared Imaging of Abdominal Aorta Blood Flow under Surgical Occlusion

William W. Lau, Homayoun Mozaffari-Naeini, Nitish V. Thakor
Department of Biomedical Engineering
Johns Hopkins University
Baltimore, MD 21205
{wlau, hmn, nthakor}@bme.jhu.edu

Abstract

This paper presents a four-wavelength near-infrared imaging system that can assist surgeons with intraoperative monitoring and imaging of blood flow of the vessel being occluded. The algorithm for this system, based on the Beer-Lambert law, calculates the relative concentrations of deoxyhemoglobin, oxyhemoglobin and water, which are the major NIR absorbers in tissues. Regional blood volume and oxygen saturation can be determined from these measurements. This proof-of-concept study investigated the utility of the algorithm on detecting rat infrarenal abdominal aortic blood flow subjected to various degrees of occlusion. The images provided a good visualization of the aorta because of the high concentration of oxyhemoglobin in the blood stream. The imager was able to detect when blood flow was completely stopped. Average intensity values of the blood volume images correlated well with the laser Doppler recordings.

1. Introduction

In many surgical procedures that require vascular manipulation, such as in bypass surgery for abdominal aortic aneurysm, temporary blood vessel occlusion is often needed. The force applied on the vessel to halt blood flow varies from surgeon to surgeon, since the amount of force needed is a subjective judgment determined by the surgeon's perception and experience. Consequently, excessive forces may be unintentionally applied, resulting in trauma to the vessel walls, particularly to the delicate endothelial cells. Damage to the endothelium can lead to a number of complications, including arterial stenosis and atherosclerosis [1].

Blood flow in the vessel being occluded can be monitored by a laser-Doppler flowmeter to prevent excessive forces being applied after the flow has stopped, and to signal if compromised blood flow occurs during the occlusion. However, the procedure is usually preformed without knowing the state of collateral circulations and the duration of safe occlusion. Risk of the surgery may reduce significantly if surgeons have the ability to visualize blood flow in not only the vessel itself but its distribution beds as well. Scanning laser-Doppler can be used to obtain two-dimensionally-resolved perfusion map by moving a probe across the field of interest, but this technique has limited temporal and spatial resolution due to the need to mechanically scan the probe.

Near-infrared (NIR) spectroscopy has been successfully applied in many clinical areas including breast cancer detection [2-4], skin hydration analysis [5-6], and functional brain imaging [7-9]. NIR imaging is a noninvasive, risk-free technique that can directly assess tissue perfusion and vascular patency by measuring light backscattered from the tissues from which

Proceedings of the 17th IEEE Symposium on Computer-Based Medical Systems (CBMS'04)
1063-7125/04 $ 20.00 © 2004 IEEE

the images are derived. Variations in light intensity are proportional to the difference in concentrations of a number of NIR absorbing compounds. Changes in total hemoglobin concentration are indicative of the variation of regional blood volume. Moreover, the strength of NIR imaging over laser-Doppler is that oxygen saturation of the blood can be determined readily through the measurement of oxyhemoglobin and deoxyhemoglobin concentrations.

Unlike many other multispectral imaging techniques that operate on huge data sets, the algorithm presented in this paper requires only four images taken at different wavelengths to solve for the chromophore concentrations. With this small number of images, it is possible to take one snapshot image and split it into four monochromic images using a set of beam splitters and interference filters. Images can be processed in real-time to provide immediate guidance for surgery. Intraoperative interventions can be carried out promptly in case of any complications so that irreversible damages can be prevented.

Biological tissues are very complex turbid media. When photons enter a tissue, they are usually scattered multiple times before either being absorbed by a chromophore or exiting the medium [10]. Their interactions are difficult to be determined precisely. The purpose of the present study is to investigate the utility of this relatively simple algorithm on infrarenal abdominal aortic blood flow subjected to various degrees of occlusion.

2. Materials and Methods

2.1. Experimental procedures

Animal care and experimental procedures were conducted following the guidelines of the Institutional Animal Care and Use Committee. Sprague-Dawley rats (n=3, 320-355 g) were anesthetized with an intraperitional injection of ketamine-xylazine (87/13 mg/kg). Additional supplements were administered as needed to maintain a constant level of anesthesia. Following a midline laparotomy, the abdominal contents were exteriorized by medial visceral rotation and the infrarenal abdominal aorta was isolated. A pair of surgical forceps was placed perpendicularly to vessel axis. Blood flow caudal to the forceps was continuously monitored by a laser-Doppler flowmeter (PeriFlux 4001, Perimed, Sweden).

A NIR-sensitive cooled charge-coupled device camera (SensiCam SVGA, Cooke, Auburn Hills, MI) was mounted on a microscope (OPMI1-H, Zeiss, Germany) placed approximately 17 cm above the exposed abdomen. A 10-V halogen lamp in the microscope was used to illuminate the field. A mechanical filter wheel (500-HF110, Prior Scientific, Rockland, MA) was fitted to the camera to house four bandpass interference filters. Their wavelengths were 701, 766, 802, and 830 nm with a bandwidth of 10 nm.

The forceps were slowly closed upon the abdominal aorta through five occlusion levels. In each step after the blood flow returned to steady state, three images of each wavelength were taken. The first image set (level 1) was a baseline taken without applying any force on the vessel. The next four sets were taken with the forceps at approximately 20, 50, 100, and 110% (levels 2-5, respectively) of the minimal displacement it needed to effectively stop the blood flow. Subsequently, the forceps was released and images were taken again at occlusion levels 1 through 3. The images had a size of 640 x 512 pixels with a 12-bit dynamic range and an exposure time of 60 ms. With this arrangement, each pixel corresponded to an area of 9.4 x 9.8 μm^2.

2.2. Image analysis

As a first step, raw images of each wavelength taken at each occlusion level were averaged to reduce the influence of random noises. A small area was selected to be the region of interest for further processing. This area was median-filtered using a 5x5 window to remove any isolated extreme values. Because of uneven surface illumination and detector response, logarithmic residual correction (LRC) was employed to subtract estimated topographical and illumination factors from the data [11]. The data set ($X_{\lambda,ij}$) was a product of the system response to specific wavelengths (I_λ), topography of the scene (T_{ij}), and the response of the tissue itself ($R_{\lambda,ij}$). This relationship can be represented by:

$$X_{\lambda,ij} = T_{ij} I_\lambda R_{\lambda,ij} \tag{1}$$

To extract $R_{\lambda,ij}$ from $X_{\lambda,ij}$, the method mean centered the images over both the image pixels and the wavelengths. The result was an approximation of the tissue response, calculated by the following equation:

$$\log\left(R_{\lambda,ij}\right) = \log\left(X_{\lambda,ij}\right) - \frac{1}{N}\sum_i \log\left(X_{\lambda,ij}\right) - \frac{1}{M}\sum_j \log\left(X_{\lambda,ij}\right) + \frac{1}{NM}\sum_{ij} \log\left(X_{\lambda,ij}\right) \tag{2}$$

where N equals to the total number of pixels within an image and M equals to the number of wavelengths used.

Evaluation of the relative concentration of each tissue chromophore was based on the Beer-Lambert law. The absorbance value at each pixel, $A_{\lambda,ij}$, was obtained by subtracting $\log(R_{\lambda,ij})$ from the maximum $\log(R_\lambda)$ among all the data sets. The resulting data cube was a three-dimensional array, combining both spatial and spectral information.

In the NIR spectrum, the primary absorbers of light are deoxyhemoglobin (deoxy-Hb), oxyhemoglobin (oxy-Hb), and water. With knowledge of accurate spectra of these chromophores over the four selected wavelengths, the concentrations of these chromophores can be assessed. The absorbance A_λ at a specific wavelength λ contributed by each chromophore is proportional to its concentration C, its absorptivity ε at that wavelength, and the optical pathlength L, which is an unknown quantity because of the complexity of scattering within the tissue. To determine the relative concentrations of each chromophore, the pathlength was assumed to be constant for all four wavelengths. The two types of unknowns were combined into a single variable. The algorithm was constructed mathematically as the following:

$$A = (C_{deoxy}L \times \varepsilon_{deoxy}) + (C_{oxy}L \times \varepsilon_{oxy}) + (C_{water}L \times \varepsilon_{water}) \tag{3}$$

The component concentrations were evaluated independently for each pixel in the image cube using least squares fitting with non-negativity constraints. Relative blood volume was acquired by the summation of deoxy-Hb and oxy-Hb concentrations.

3. Results

The algorithm was written in MATLAB. The images were processed on a desktop computer with a 2.33-GHz P4 processor and 512 megabytes of memory. Figure 1 shows the relative deoxy-Hb, oxy-Hb, and total hemoglobin concentrations of the abdominal

aorta under no occlusion and total occlusion. Specular reflections and the region in contact of the forceps were excluded from analysis. These images provide a good visualization of the aorta because of the high concentration of oxy-Hb in the arterial blood. They also clearly indicate the differences before and after occlusion.

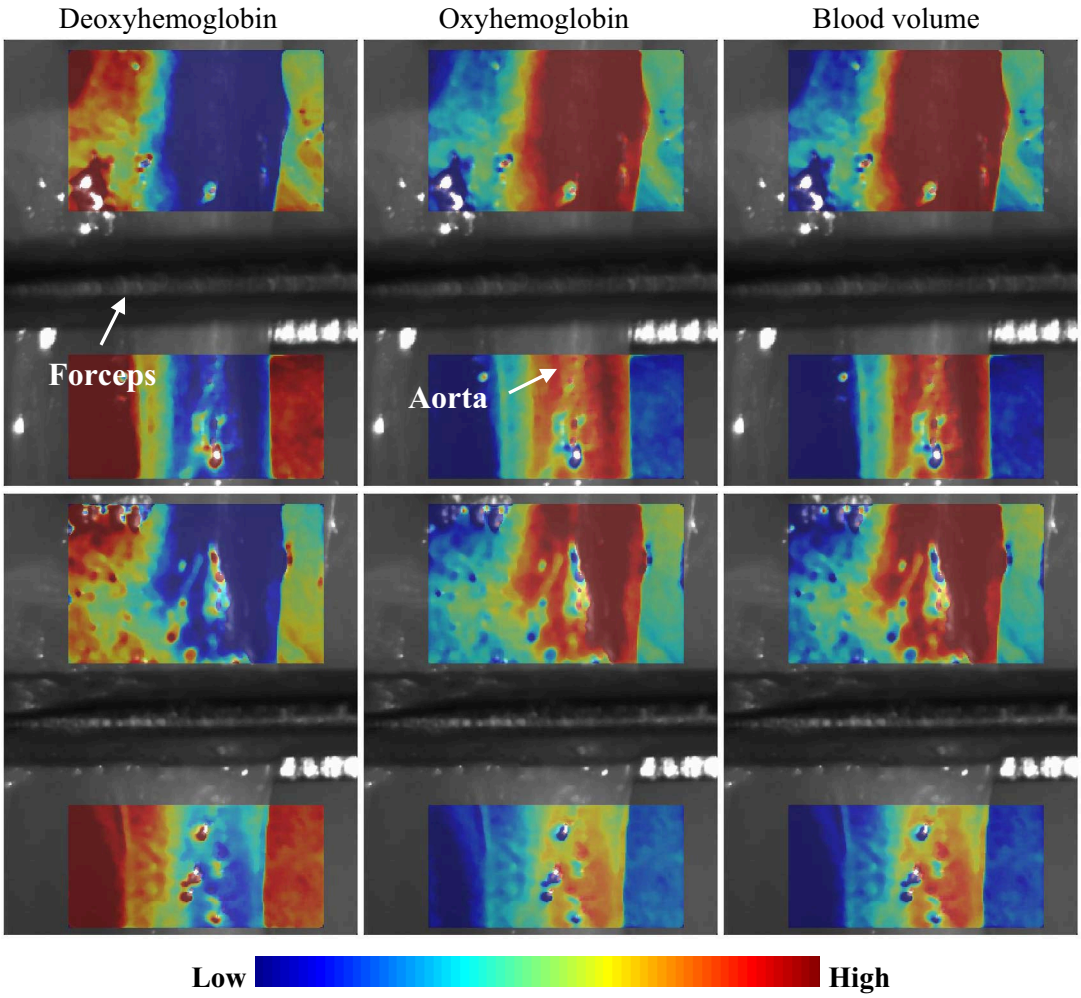

Figure 1. Relative deoxy-Hb, oxy+Hb, and (deoxy-Hb + oxy-Hb) concentration maps overlaid on the raw images for no occlusion (top) and total occlusion (bottom). Total hemoglobin concentration is proportional to blood volume. Bottom = caudal.

Blood volume changes in a region of the abdominal aorta caudal to the occlusion site are illustrated in figure 2. To compare the image data with the laser-Doppler measurements, values obtained from the two techniques are normalized by the respective baseline readings. Figure 2b shows that blood volume is linearly-dependent on the degree of occlusion whereas blood flow is exponentially-dependent. When the forceps was released progressively after occlusion level 5, blood flow recovered but not completely as compared to the measurements obtained prior to total occlusion. Oxygen saturation did not vary significantly among different occlusion levels. Average SO_2 for the three trials are 85.9 ± 1.4% (95% C.I.), 90.3% ± 0.5% and 98.2 ± 0.9%.

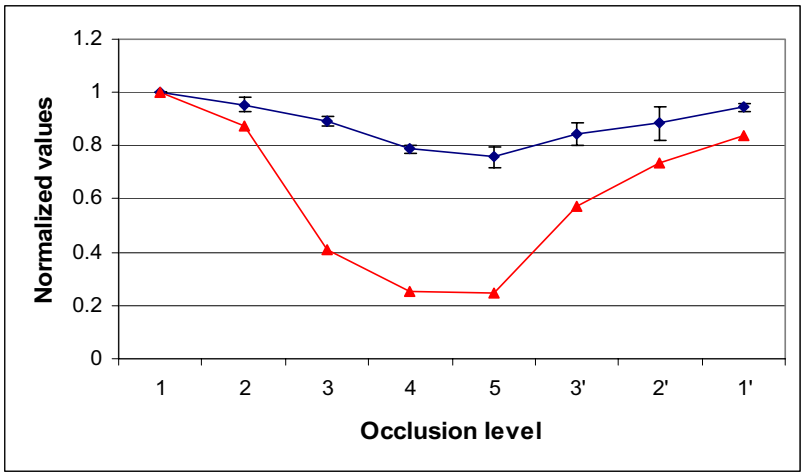

(a)

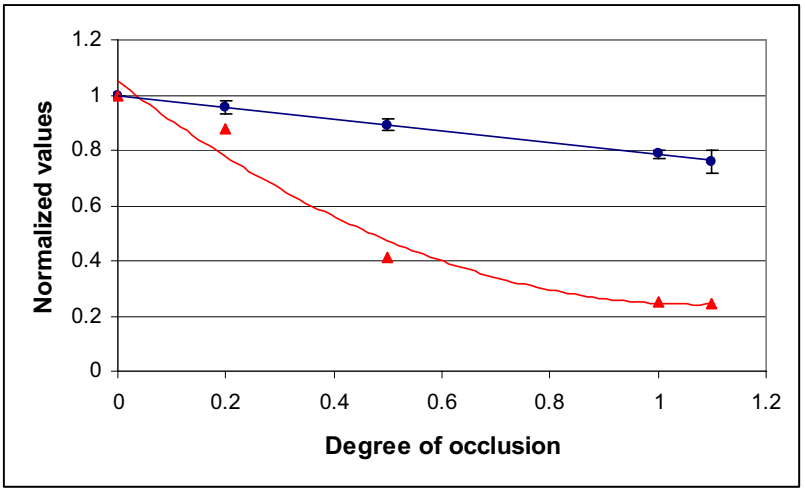

(b)

Figure 2. Mean image intensities of the occluded abdominal aorta (blue circles) derived from the blood volume maps for each occlusion level averaged over three trials and the corresponding laser-Doppler measurements (red triangles) obtained from one trial. Prime marks in (a) denote occlusions during the release of the forceps. The degree of occlusion in (b) is normalized by the minimal forceps displacement for total occlusion. Error bars denote standard errors.

4. Discussion

The results outlined above support the viability of monitoring blood flow and tissue perfusion with only four wavelengths. Blood flow changes due to various degrees of occlusion are clearly revealed in the images, although laser-Doppler flowmetry appear to be more sensitive to these changes. The dependence of blood flow and blood volume on the degree of occlusion is inconclusive because of the small sample size.

After the blood flow was completely occluded, further displacement of the forceps did not result in a significant change in blood volume values. This helped the user to determine what the minimum occlusive force was. When the forceps was fully released, blood volume returned to approximately 95% of the baseline value. This may indicate damages to the blood vessel wall even though the maximum degree of occlusion applied was only 10% higher than what was necessary to stop the blood flow. In addition, tissue

perfusion and blood oxygen saturation level did not vary considerably within each trial. The SO_2 measurements reported here reflect the oxygenation state of the arterial blood as well as the tissues underneath the vessel. Inter-subject variability can be due to a number of factors including inherent physiological differences and the inability of LRC to completely eliminate artifacts caused by the uneven surface geometry and illumination.

Tissue scattering is a very complicated phenomenon. To ensure the computational efficiency of the algorithm, it is assumed that the wavelength-dependent optical pathlength is uniform for all four wavelengths. Since a relatively narrow range of wavelengths has been used in the study, the effect of not compensating for the wavelength dependence of tissue scattering is minimal. It is important to note that motion artifacts due to blood flow pulsations also reduce the spatial resolution of the images. The effect is most noticeable at the edges of the aorta.

In conclusion, although this technique does not provide quantitative measurements, it gives surgeons more information on what is happening at the surgical site, allowing them to accomplish blood vessel occlusion without applying excessive force and monitor the spatio-temporal variations in oxygenation of the surrounding tissues. Future works include refinements of the system to take all four images simultaneously and to process the data in real-time. Other applications, such as tissue hydration assessment, will also be investigated. Upon further developments, this NIR imaging system will enable surgeons to perform complex vascular procedures and other surgeries with more confidence and reliability.

Acknowledgement

Partial funding for this work was provided by the NSF.

References

[1] Carmeliet P. and Collen D. "Molecular analysis of blood vessel formation and disease", Am J Physiol Heart Circ Physiol., 1997, 273: pp. H2091-H2104.

[2] Srinivasan S., Pogue B.W., et al. "Interpreting hemoglobin and water concentration, oxygen saturation, and scattering measured in vivo by near-infrared breast tomography", Proc Natl Acad Sci USA., 2003, 100(21): pp. 12349-54.

[3] Pogue B.W., Poplack S.P., et al. "Quantitative hemoglobin tomo-graphy with diffuse near-infrared spectroscopy: pilot results in the breast", Radiology, 2001, 218: pp. 261–6.

[4] Shah N., Cerussi A., et al. "Noninvasive functional optical spectroscopy of human breast tissue", Proc Natl Acad Sci USA, 2001, 98(8): pp. 4420–5.

[5] Sowa M.G., Payette J.R., and Mantsch H.H. "Near-infrared spectroscopic assessment of tissue hydration following surgery", J Surg Res, 1999, 86(1): pp. 62-9.

[6] Attas M., Hewko M., et al. "Visualization of cutaneous hemoglobin oxygenation and skin hydration using near-infrared spectroscopic imaging", Skin Res Technol., 2001, 7(4): pp. 238-45.

[7] Benaron D.A., Hintz S.R., et al. "Noninvasive functional imaging of human brain using light", J Cereb Blood Flow Metab., 2000, 20(3): pp. 469-77.

[8] Toronov V., Franceschini M.A., et al. "Near-infrared study of fluctuations in cerebral hemodynamics during rest and motor stimulation: temporal analysis and spatial mapping", Med Phys., 2000, 27(4): pp. 801-15.

[9] Devor A., Dunn A.K., et al. "Coupling of total hemoglobin concentration, oxygenation, and neural activity in rat somatosensory cortex", Neuron., 2003, 39(2): pp. 353-9.

[10] Arnoldussen M.E., Cohen D., et al. "Consequences of scattering for spectral imaging of turbid biologic tissue", J Biomed Opt., 2000, 5(3): pp. 300-6.

[11] Mansfield J.R., Sowa M.G., et al. "Tissue viability by multispectral near infrared imaging: a fuzzy C-means clustering analysis", IEEE Trans Med Imaging, 1998, 17(6): pp. 1011-8.